Reflective optical vortex generators with ultrabroadband self-phase compensation

Han Cao,[a,b] **Guangyao Wang,**[a] **Lichao Zhang,**[b] **Qinggui Tan,**[c] **Wei Duan,**[d,*] **and Wei Hu**[ORCID][a,*]

[a]Nanjing University, College of Engineering and Applied Sciences, National Laboratory of Solid State Microstructures, Key Laboratory of Intelligent Optical Sensing and Manipulation, Nanjing, China
[b]Nanhui Institute of Intelligent Optical Sensing and Manipulation, Nanjing, China
[c]China Academy of Space Technology, National Key Laboratory of Science and Technology on Space Microwave, Xi'an, China
[d]Beihang University, School of Instrumentation and Optoelectronic Engineering, Beijing, China

Abstract. The explosive growth of information urgently requires extending the capacity of optical communication and information processing. Orbital-angular-momentum-based mode division multiplexing (MDM) is recognized as the most promising technique to improve the bandwidth of a single fiber. To make it compatible with the dominant wavelength division multiplexing (WDM), broadband equal high-efficient phase encoding is highly pursued. Here, we propose a twisted-liquid-crystal and rear-mirror-based design for ultrabroadband reflective planar optics. The backtracking of the light inside the twisted birefringent medium leads to an achromatic phase modulation. With this design, a single-twisted reflective q-plate is demonstrated to convert a white beam to a polychromatic optical vortex. Jones calculus and vector beam characterization are carried out to analyze the broadband phase compensation. A dual-twisted configuration further extends the working band to over 600 nm. It supplies an ultrabroadband and reflective solution for the WDM/MDM-compatible elements and may significantly promote advances in ultrabroadband planar optics.

Keywords: liquid crystal polymers; optical vortex; geometric phase; ultrabroadband.

1 Introduction

Currently, advanced photonics applications such as 5G/6G communication, Internet of Things, optical computing, augmented/virtual reality, and holographic displays drastically increase the demand for information bandwidth. Photonic informatics exhibits superiority to electronic techniques due to its intrinsic multidimensional and large-scale parallel processing. At present, wavelength division multiplexing (WDM) is the dominant way to extend the bandwidth of a single fiber. New multiplexing techniques have continued to be explored to further tap the potential of photons. Among various approaches, space division multiplexing is recognized as the most promising solution for next-generation optical communications.[1] Orbital angular momentum (OAM)-based mode division multiplexing (MDM) has attracted particular attention due to its theoretically infinite number of OAM channels corresponding to infinite orthogonal optical vortex (OV) states.[2,3] OV, featured by a helical phase front, carries OAM of $m\hbar$ per photon, where m is the topological charge, meaning how many twists the light does in one wavelength, and $\hbar$ is the reduced Planck constant.[4–6] Adopting OAM as separate channels will dramatically enhance the capacity of optical comunications.[7] To make the OAM-based MDM compatible with WDM, broadband equal high-efficient OAM encoding and processing are thus highly pursued. The convenient method for broadband high-efficient spatial phase modulation of compact size and high quality is still challenging, hindering high-speed processing, reliable transmission, and versatile utilization of massive information.

In recent years, planar optics composed of plasmonic or dielectric artificial nanostructures has substantially advanced modern optics by overcoming the bulky size of conventional deflective optics.[8–10] Due to the intrinsic broadband birefringence and diverse external field responsiveness, liquid crystals (LCs) are regarded as yet another top contender for planar

*Address all correspondence to Wei Duan, wduan@buaa.edu.cn; Wei Hu, huwei@nju.edu.cn

optics.[11] By precisely manipulating the tilt angle of LC directors in LC on silicon[12] or the azimuthal angle in geometric phase LC optics,[13] one can spatially modulate the phase front of light. Their maximum efficiencies always occur at the half-wave condition, and the efficiency drops significantly when the wavelength deviates. Helical structures are introduced to LC planar optics for broadband high-efficient phase modulation.[14,15] Mirror-symmetric multi-twist configurations endow transmissive LC planar optics with an ultrabroadband working frequency range.[16–18] The technique still suffers from its fine process and complicated fabrication. Cholesteric LC (CLC), featured by a periodic helical director distribution, is adopted in reflective planar optics due to its broadband Bragg–Berry phase modulation.[19–22] By this means, reflective OV processors are demonstrated, and up to 25 individual OAM modes are extracted equally efficiently over a wavelength of 116 nm.[23] A wash-out-refill technique is further adopted to electrically shift the whole reflection band and to realize OAM processing with ultrabroadband tunability.[24] Heliconical cholesteric is introduced for ultrabroadband tunable narrow bandgap planar optics. The OV generator, beam deflector, and off-axis lens with a customizable working band in the shifting range from 1550 to 380 nm are demonstrated.[25] The bandwidth of the above CLC planar optics is restricted to ~100 nm. Additionally, the geometric phase is selectively encoded to the circular polarization (CP) with the same handedness as the helical structure, hindering the practical application of such devices. If the above problems are solved satisfactorily, WDM/MDM compatible elements may be inspired.

We propose a new design for reflective planar optics with high efficiency in an ultrabroadband and conjugated phase modulation for opposite spins. It is composed of a photopatterned LC monolayer of specifically designed thickness and twisted angle and a rear mirror. Due to the backtracking of the wave vector caused by the mirror, a perfectly mirror-symmetric dual-twist configuration is formed. Jones calculus analysis indicates that self-phase compensation is realized for polychromatic incident light. A q-plate with the proposed design converts a white beam to an OV. Moreover, topological charge reversal is demonstrated by altering the incident spins. By adding another twisted layer, a forked polarization grating (FPG) is demonstrated with a working band covering both the visible and near-IR regions. It overcomes the shortcomings of conventional CLC elements and establishes a practical solution for ultrabroadband reflective planar optics, which may promote advances in WDM/MDM-compatible communications and many other photonic applications.

2 Designs and Principles

Figure 1(a) schematically illustrates the configuration of the proposed twisted LC cell. It is composed of a twisted LC layer for self-phase compensation and a rear mirror for wave vector backtracking. The function of the device can be calculated by the Jones calculus. Omitting the constant phase introduced by specular reflection, the Jones matrix of the device can be depicted as

$$\mathbf{T} = \mathbf{R}(-\alpha)\mathbf{M}(d,-\phi)\mathbf{M}(d,\phi)\mathbf{R}(\alpha), \quad (1)$$

where $\mathbf{R}$ is the coordinate rotation matrix, α is the rotation angle of the entrance director with respect to the x axis, $\mathbf{M}(d,\phi)$ is the Jones matrix of the twisted LC layer[26] with thickness d, the twist angle ϕ, and $\mathbf{M}(d,-\phi)$ is the Jones matrix of the twisted LC for specular light. By adding more Jones matrix pairs, one can simulate the output field of a multi-twisted cell. All Jones matrices are depicted in the same coordinate. After a series of mathematical expansions (see Supplementary Material), the above equation can be expressed as

$$\mathbf{T} = \left\{ \cos^2 X + \left[\phi^2 - \left(\frac{\Gamma}{2}\right)^2 \right] \frac{\sin^2 X}{X^2} \right\} \begin{pmatrix} 1 & 0 \\ 0 & 1 \end{pmatrix}$$
$$- i\Gamma \frac{\sin X}{X} \sqrt{\cos^2 X + \phi^2 \frac{\sin^2 X}{X^2}} \begin{bmatrix} \cos(2\alpha - \varphi) & \sin(2\alpha - \varphi) \\ \sin(2\alpha - \varphi) & -\cos(2\alpha - \varphi) \end{bmatrix},$$
$$(2)$$
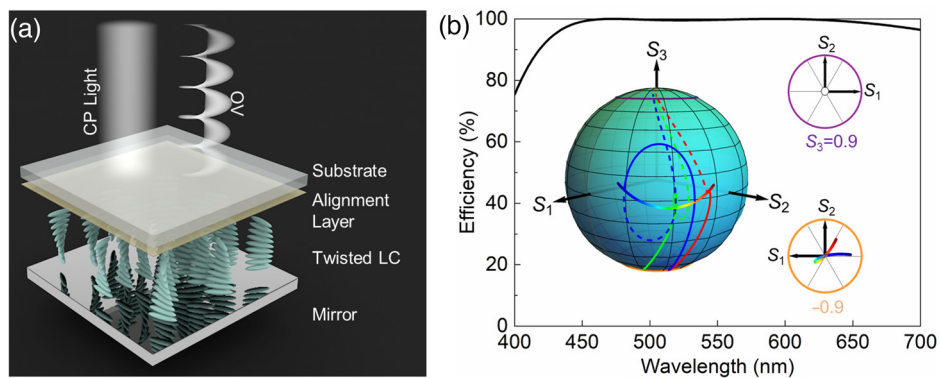
Fig. 1 (a) Schematic illustration of a patterned twisted LC cell and its function as an achromatic OV generator. (b) Wavelength-dependent CP conversion efficiency of an optimized structure and polarization evolutions of different wavelengths on the Poincaré sphere. The wavelength range from 440 to 660 nm is considered and the evolution trajectories of three typical wavelengths, 450 nm (blue), 530 nm (green), and 630 nm (red), are presented. Dashed and solid lines reveal the trajectories before and after backtracking. Input polarization on the north pole and output polarization around the south pole are exhibited as insets.

$$e^{i\varphi} = \frac{\cos X - i\phi \frac{\sin X}{X}}{\sqrt{\cos^2 X + \phi^2 \frac{\sin^2 X}{X^2}}}, \qquad (3)$$

where $X = \sqrt{(\Gamma/2)^2 + \phi^2}$; $\Gamma = 2\pi \Delta n \, d/\lambda$ is phase retardation; Δn and λ are the birefringence of the LC and incident wavelength, respectively; and φ is a geometric phase induced by the twisted structure. Considering CP incidence described as $|\mathbf{E}_{in}\rangle = \frac{1}{\sqrt{2}}\begin{pmatrix} 1 & \pm i \end{pmatrix}^{T}$, the output field is expressed as

$$\begin{aligned} |\mathbf{E}_{out}\rangle &= \mathbf{T} \cdot |\mathbf{E}_{in}\rangle \\ &= \frac{1}{\sqrt{2}} \left\{ \cos^2 X + \left[\phi^2 - \left(\frac{\Gamma}{2} \right)^2 \right] \frac{\sin^2 X}{X^2} \right\} \begin{pmatrix} 1 \\ \pm i \end{pmatrix} \\ &\quad - i \frac{\Gamma}{\sqrt{2}} \frac{\sin X}{X} \sqrt{\cos^2 X + \phi^2 \frac{\sin^2 X}{X^2}} e^{\pm i(2\alpha - \varphi)} \begin{pmatrix} 1 \\ \mp i \end{pmatrix}. \end{aligned} \quad (4)$$

When the incident CP is handedness-converted, the light carries a geometric phase twice the value of α. Moreover, conjugated phases are encoded for opposite spins. The CP conversion efficiency is given as

$$\eta = \Gamma^2 \frac{\sin^2 X}{X^2} \left(\cos^2 X + \phi^2 \frac{\sin^2 X}{X^2} \right). \qquad (5)$$

We set a target band from 440 to 660 nm and further consider $\Delta n = 0.132 + 9964/\lambda^2$ to fit the Δn dispersion of the LC used. Then, we calculate using MATLAB to find the optimal structure parameters (d, ϕ) to acquire the maximum η within the band. The calculated result for $d = 1.46 \mu m$ and $\phi = \pm 69.2$ deg is shown in Fig. 1(b). High η near 100% is achieved in the range from 450 to 650 nm, due to the perfect polychromatic phase compensation introduced by the specific twist structure.

We calculated the polarization evolution in the wavelength range from 440 to 660 nm for the twisted LC cell with the above optimized parameters. The incident is set as a right-handed CP light, i.e., the north pole on the Poincaré sphere. According to the backtracking optical path, the evolution is naturally divided into two different parts. One is from the north pole to regions around the equator, and the other is the continuous evolution toward the south pole, as shown in Fig. 1(b). The evolution trajectories of three typical wavelengths, 450 nm (blue), 530 nm (green), and 630 nm (red), are selected as examples to visually reveal the self-phase compensation. Dashed and solid lines reveal the trajectories before and after backtracking, respectively. Light of different wavelengths experiences distinct trajectories and creates a knot around the north pole. The trajectories are formed due to the wavelength-dependent combination of the dynamic phase and geometric phase, leading to the self-compensation effect. All the points on the knot are very close to the south pole, perfectly matching the curve of the wavelength-dependent CP conversion efficiency.

3 Results and Discussions

By rationally designing the initial LC director distribution of the self-phase compensated wave plate, arbitrary phase modulation can be realized. The general fabrication process is briefly listed below. First, the predesigned pattern is recorded to a spin-coated azo-dye SD1[27] (NCLCP, China) layer via photopatterning.[13] Second, the solution of LC polymer NC-M-LCP1 (28 wt%,

NCLCP, China) mixed with chiral dopant S811 (0.23 wt%, NCLCP, China) is spin-coated onto the SD1 layer at 1500 rpm for 80 s and then is UV-cured immediately. Third, the twisted-LC film is stuck to a mirror (OMM1-S1, JCOPTIX, China) using optical adhesive NOA 63 (Norland Products Inc.) and cured under UV. Finally, a supercontinuum laser (SuperK EVO, NKT Photonics, Denmark) is adopted for characterization, which is filtered by an acousto-optic tunable filter (SuperK SELECT, NKT Photonics, Denmark) to selectively output arbitrary wavelength in the range from 410 to 1200 nm. Microscopy observations are carried out on a polarization optical microscope (POM, Nikon 50i, Japan) with crossed polarizers.

For demonstration, a q-plate is fabricated, whose initial director distribution is depicted by $\alpha = q\theta$, where $q = m/2$ and $\theta = \mathrm{atan}(y/x)$. Here, we set $q = 0.5$, and the encoded phase is revealed in Fig. 2(a). Figure 2(b) shows the micrograph of the q-plate under a POM. Its centrosymmetric color variation is attributed to the interference color caused by the optical rotatory dispersion of the sample. Figure 2(c) exhibits the optical setup for the OV characterization. Figure 2(d) shows the generated OVs for blue, green, and red lasers, respectively. An astigmatic transformation method[28] is adopted for the detection of m. The number and tilt direction of the dark stripe converted by an OV in the focal plane of a cylindrical lens reveal the value and sign of carried topological charge, respectively. Gaussian beams with orthogonal CPs are both completely converted to donut-like OV beams. Only one dark stripe is observed for OAM detection, suggesting $|m| = 1$. The different tilt directions for opposite CPs imply that conjugated phases are encoded to beams with opposite spins. Dark centers are observed in all generated OVs, indicating the polychromatic highly efficient phase modulation of the proposed design.

When a linearly polarized (LP) light is incident on the self-phase compensated q-plate, the two generated OVs with opposite m recombine to form a vector beam. Its space-variant polarization distribution is expressed by $m\theta + \beta(\lambda)$. $\beta(\lambda)$ is an additional polarization rotation introduced by φ in Eq. (2). φ shows an intensive wavelength dependency and plays a vital role in the self-phase compensation of the twisted LC. Figure 3 shows the characterizations of vector beams generated by the self-phase compensated q-plate with $q = 0.5$. The vector beams exhibit the same polarization order of 1, while from blue to red, β is rotated clockwise, as revealed by the different intensity distributions recorded after an analyzer. The wavelength-dependent rotation of the dark stripe indicates the space-variant polarization distribution of generated vector beams with different wavelengths, which is attributed to the combination of optical activity and birefringence dispersion introduced by the twisted LC. This phenomenon is consistent with the lateral dispersion of different wavelengths around the equator on the Poincaré sphere. This verifies the existence of φ and endows the device with a wavelength-dependent optical axis. The generation of a white-light vector beam is also demonstrated. The light from a white-light-emitting diode (LEM-W2, JCOPTIX, China) is converted to a donut vector beam with a dark center. It vividly shows the high mode conversion efficiency over the whole visible band. The colorful lobes indicate the continuous rotation of the optical axis corresponding to the variation of wavelength.

To further extend the bandwidth, a dual-twisted LC structure, as shown in Fig. 4(a), is introduced (see Supplementary Material). We design a dual-twisted FPG with $d_1 = 2.25 \mu m$, $d_2 = 1.06 \mu m$, $\phi_1 = 102.5$ deg, and $\phi_2 = -66.9$ deg. Its initial
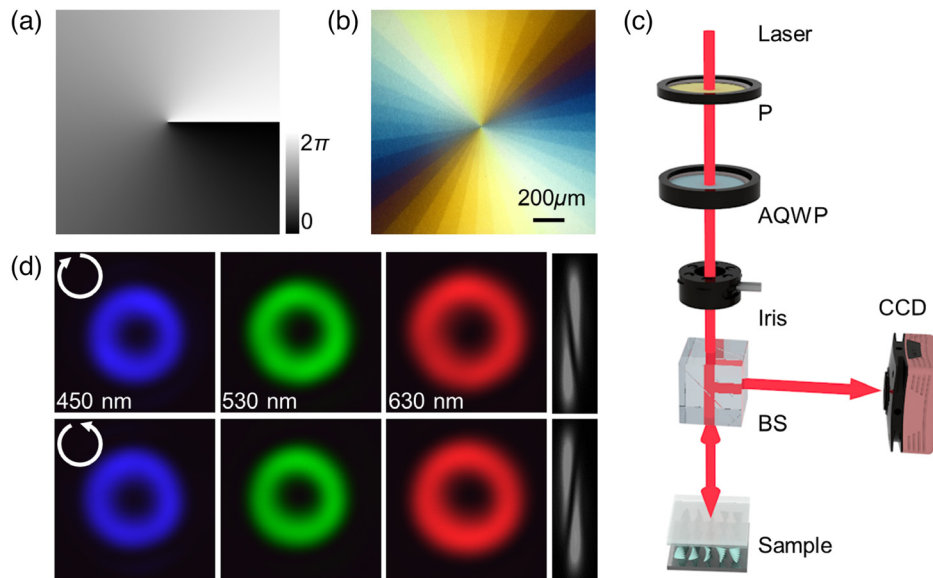
Fig. 2 Polychromatic OV generation based on a self-phase compensated q-plate. (a) Phase diagram and (b) micrograph of the q-plate with $q = 0.5$. (c) Optical setup for the OV characterization. P, polarizer; AQWP, achromatic quarter-wave plate; BS, beam splitter. (d) Corresponding polychromatic OVs and OAM detections.
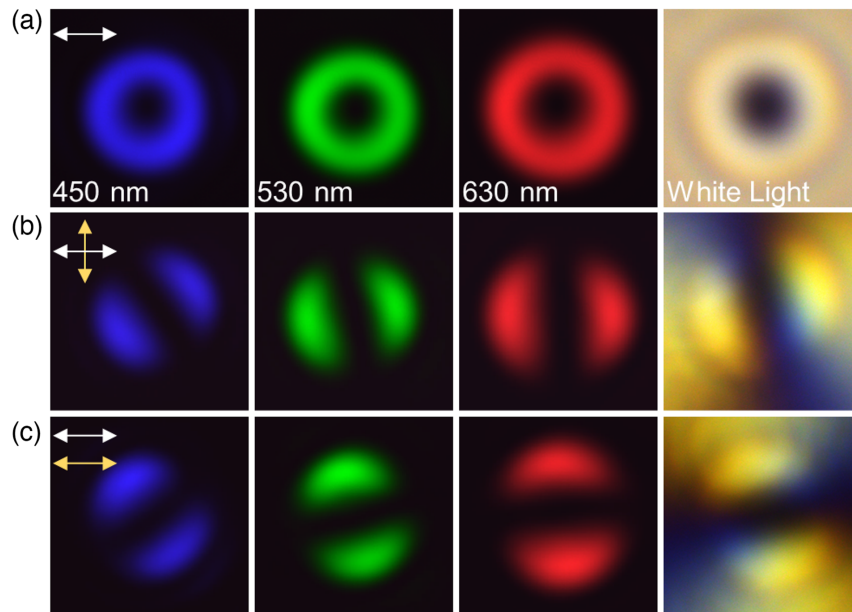
Fig. 3 (a) Vector beams generated by the self-phase compensated q-plate with $q = 0.5$ for LP incidence. Vector beams detected with an analyzer (b) crossed and (c) parallel to the polarizer. White and yellow arrows denote the directions of polarizer and analyzer, respectively. The incident wavelengths are labeled correspondingly.

LC director distribution is given by $\alpha_{FPG} = q\theta + \pi x/\Lambda$, where the first term represents a q-plate and the second term represents a polarization grating.[29] Figure 4(b) shows the phase diagram of an FPG with $q = 1$. Figure 4(c) reveals the micrograph of the fabricated FPG. It divides the opposite CPs into two separate orders, which are OVs with opposite m. The diffraction efficiency is defined as the intensity ratio of the objective diffraction orders to the total transmission, i.e., Fresnel reflection is not considered. The calculation reveals a high efficiency near 100% in the wavelength range from 400 to 1000 nm, while the measured diffraction efficiency reaches $96.4\% \pm 1.44\%$ in the range from 425 to 1000 nm, as shown in Fig. 4(d). An optical power meter with properly sized apertures is adopted to measure the intensity, and then the efficiency is calculated correspondingly.
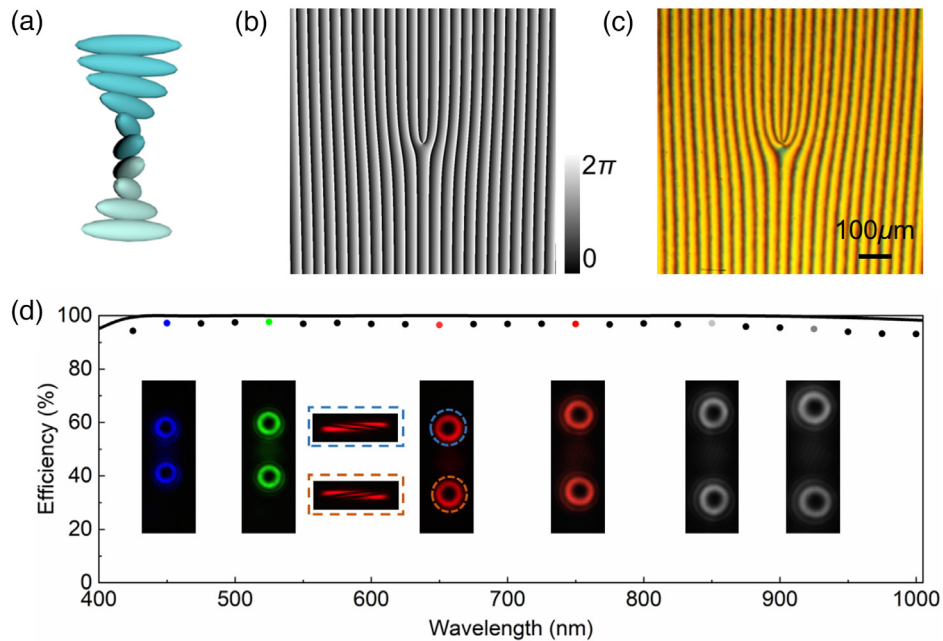
Fig. 4 (a) Illustration of the dual-twisted LC configuration. (b) Phase diagram and (c) micrograph of a dual-twisted FPG with $m = 2$. (d) Simulated (solid line) and detected (dots) wavelength-dependent diffraction efficiencies. Insets reveal the generated donut OVs of wavelengths the same as the dots marked in the same color and the insert dash rectangles present the astigmatic transformation results of the 650-nm OVs.

Both the simulation and the detection exhibit an ultrabroadband diffraction efficiency of the dual-twisted FPG. Corresponding selected diffraction patterns are illustrated in Fig. 4(d). Donut-like OVs with $m = \pm 2$ are observed, while the 0th orders are negligible in the whole range, further verifying the ultrabroadband high efficiency.

Compared to CLC planar optics, the working bands of the proposed reflective OV generators are drastically extended. For single-twist and dual-twist configurations, the band ($\eta > 95\%$) reaches 250 and 600 nm, respectively, and the latter is almost 10 times wider than the bandwidth of traditional CLCs. For vivid demonstration reason, here, the structure is optimized for the visible region. The working band can be easily shifted by tailoring the parameters of the twisted structure. By properly increasing the thickness of the LC, the WDM/MDM-compatible elements can be realized in the commonly used C and L bands. The self-phase compensated devices encode conjugated phases to light of different spins. The backtracking optical path enables the perfect mirror symmetry of the twisted configurations, thus significantly improving the performance with a much-simplified structure and fabrication process. For single-twisted devices, the functional material is not restricted to the LC polymer. LC can be adopted as well, making the electro-optical switching of the phase modulation achievable. The self-phase compensation of proposed twisted LC devices is not limited to continuous wave (CW) lasers. It can be extended to any scalar diffraction cases, including optical fields with complex spatiotemporal structures and vortex pulses in a broad spatial spectrum.[30,31] Nowadays, structured light exploiting various hidden degrees of freedom beyond OAM light has been adopted to break the conventional capacity limit of the OAM/MDM protocol.[32,33] Fortunately, the proposed design is not restricted to OAM generation. It is suited for the arbitrary spatial phase/polarization/amplitude modulation with an ultrabroadband feature. Therefore, it provides a versatile platform even for higher-dimensional multiplexing and may be broadly used in beam steering, optical imaging, and specific optical field generation as well.

4 Conclusion

A twisted-LC and rear-mirror-based design is proposed for reflective planar optics. The backtracking of light leads to the perfect mirror-symmetry of the twist configuration and thus enables the ultrabroadband phase compensation for the incident light. A single-twisted reflective q-plate is demonstrated to convert a white beam to an OV with high efficiency. A dual-twisted configuration further extends the working band to the range from 400 to 1000 nm with a mode conversion efficiency of over 95%. Such planar optics encodes conjugated phases to orthogonal spins. It supplies a practical platform for ultrabroadband reflective planar optics, which may inspire many advanced photonic applications, especially WDM/MDM-compatible elements for optical communications.

References

1. H. Huang et al., "100 Tbit/s free-space data link enabled by three-dimensional multiplexing of orbital angular momentum, polarization, and wavelength," *Opt. Lett.* **39**(2), 197–200 (2014).
2. L. Allen et al., "Orbital angular-momentum of light and the transformation of Laguerre–Gaussian laser mode," *Phys. Rev. A* **45**(11), 8185–8189 (1992).
3. Y. Yan et al., "High-capacity millimetre-wave communications with orbital angular momentum multiplexing," *Nat. Commun.* **5**, 4876 (2014).
4. L. Marrucci, C. Manzo, and D. Paparo, "Optical spin-to-orbital angular momentum conversion in inhomogeneous anisotropic media," *Phys. Rev. Lett.* **96**(16), 163905 (2006).
5. Y. J. Shen et al., "Optical vortices 30 years on: OAM manipulation from topological charge to multiple singularities," *Light Sci. Appl.* **8**(1), 90 (2019).
6. S. Slussarenko et al., "Tunable liquid crystal q-plates with arbitrary topological charge," *Opt. Express* **19**(5), 4085–4090 (2011).
7. T. Lei et al., "Massive individual orbital angular momentum channels for multiplexing enabled by Dammann gratings," *Light Sci. Appl.* **4**, e257 (2015).
8. L. L. Huang et al., "Dispersionless phase discontinuities for controlling light propagation," *Nano Lett.* **12**(11), 5750–5755 (2012).
9. G. X. Li et al., "Spin-enabled plasmonic metasurfaces for manipulating orbital angular momentum of light," *Nano Lett.* **13**(9), 4148–4151 (2013).
10. Y. Q. Hu et al., "Electrically tunable multifunctional polarization-dependent metasurfaces integrated with liquid crystals in the visible region," *Nano Lett.* **21**(11), 4554–4562 (2021).
11. B. Y. Wei et al., "Generating switchable and reconfigurable optical vortices via photopatterning of liquid crystals," *Adv. Mater.* **26**(10), 1590–1595 (2014).
12. Z. C. Zhang, Z. You, and D. P. Chu, "Fundamentals of phase-only liquid crystal on silicon (LCOS) devices," *Light Sci. Appl.* **3**(1), e213 (2014).
13. P. Chen et al., "Liquid-crystal-mediated geometric phase: from transmissive to broadband reflective planar optics," *Adv. Mater.* **32**(27), 1903665 (2020).
14. R. Yuan et al., "Spin-decoupled transflective spatial light modulations enabled by a piecewise-twisted anisotropic monolayer," *Adv. Sci.* **9**(23), 2202424 (2022).
15. Q. M. Chen et al., "Helical structure endows liquid crystal planar optics with a customizable working band," *Adv. Quantum Technol.* **6**(2), 2200153 (2023).
16. C. Oh and M. J. Escuti, "Achromatic diffraction from polarization gratings with high efficiency," *Opt. Lett.* **33**(20), 2287–2289 (2008).
17. J. Y. Zou et al., "Broadband wide-view Pancharatnam–Berry phase deflector," *Opt. Express* **28**(4), 4921–4927 (2020).
18. W. Chen et al., "Super-broadband geometric phase devices based on circular polarization converter with mirror symmetry," *Appl. Phys. Lett.* **119**(10), 101103 (2021).
19. R. Barboza et al., "Berry phase of light under Bragg reflection by chiral liquid-crystal media," *Phys. Rev. Lett.* **117**(5), 053903 (2016).
20. M. Rafayelyan and E. Brasselet, "Bragg–Berry mirrors: reflective broadband q-plates," *Opt. Lett.* **41**(17), 3972–3975 (2016).
21. J. Kobashi, H. Yoshida, and M. Ozaki, "Planar optics with patterned chiral liquid crystals," *Nat. Photonics* **10**(6), 389–392 (2016).
22. M. Rafayelyan and E. Brasselet, "Spin-to-orbital angular momentum mapping of polychromatic light," *Phys. Rev. Lett.* **120**(21), 213903 (2018).
23. P. Chen et al., "Digitalizing self-assembled chiral superstructures for optical vortex processing," *Adv. Mater.* **30**(10), 1705865 (2018).
24. C. T. Xu et al., "Tunable band-pass optical vortex processor enabled by wash-out-refill chiral superstructures," *Appl. Phys. Lett.* **118**(15), 151102 (2021).
25. C. T. Xu et al., "Heliconical cholesterics endows spatial phase modulator with an electrically customizable working band," *Adv. Opt. Mater.* **10**(19), 2201088 (2022).
26. P. Yeh and C. Gu, *Optics of Liquid Crystal Displays*, Wiley (1999).
27. V. Chigrinov et al., "Synthesis and properties of azo dye aligning layers for liquid crystal cells," *Liq. Cryst.* **29**(10), 1321–1327 (2002).
28. V. Denisenko et al., "Determination of topological charges of polychromatic optical vortices," *Opt. Express* **17**(26), 23374–23379 (2009).
29. P. Chen et al., "Arbitrary and reconfigurable optical vortex generation: a high-efficiency technique using director-varying liquid crystal fork gratings," *Photonics Res.* **3**(4), 133–139 (2015).
30. Y. J. Shen et al., "Measures of space-time nonseparability of electromagnetic pulses," *Phys. Rev. Res.* **3**, 013236 (2021).
31. A. Zdagkas et al., "Observation of toroidal pulses of light," *Nat. Photonics* **16**, 523–528 (2022).
32. Z. S. Wan et al., "Divergence-degenerate spatial multiplexing towards future ultrahigh capacity, low error-rate optical communications," *Light Sci. Appl.* **11**, 144 (2022).
33. C. He et al., "Towards higher-dimensional structured light," *Light Sci. Appl.* **11**, 205 (2022).

Han Cao is a master's student working under the supervision of Wei HU at the College of Engineering and Applied Sciences at Nanjing University. He received his BS degree from Nanjing University of Information Science & Technology in 2020. Currently, he is working on liquid crystal planar optics.

Guangyao Wang received his BS degree from Qingdao University in 2021. He is currently working toward his MS at the College of Engineering and Applied Sciences at Nanjing University. His research interests include liquid crystal planar optics, holography, and information security.

Lichao Zhang received his master's degree from University of Shanghai for Science and Technology, Shanghai, China, in 2012. He is currently an optical engineer in charge of the research and development of liquid crystal optical products in Nanhui Institute of Intelligent Optical Sensing and Manipulation.

Qinggui Tan received his PhD in optical from the University of Electronic Science and Technology of China, Chengdu, China, in 2006. He is currently a professor with the National Key Laboratory of Science and Technology on Space Microwave, CAST. His research fields are microwave photonics, space laser communication, and optical phased array antenna.

Wei Duan is a postdoctoral research fellow supported by the "Zhuoyue" Program at Beihang University. She received her PhD from Nanjing University, Nanjing, China, in 2019. Her current research interests include liquid crystal optics and photonics.

Wei Hu is a professor at the College of Engineering and Applied Sciences, Nanjing University. He received his PhD from Jilin University, Changchun, China, in 2009. His current research interests include liquid crystal materials and optical devices.